

Journal of the Atmospheric Sciences

Weakening of tropical free tropospheric temperature gradients with global warming --Manuscript Draft--

Manuscript Number:	
Full Title:	Weakening of tropical free tropospheric temperature gradients with global warming
Article Type:	Article
Corresponding Author:	Heng Quan Princeton University Princeton, NJ UNITED STATES
Corresponding Author's Institution:	Princeton University
First Author:	Heng Quan
Order of Authors:	Heng Quan Yi Zhang Stephan Fueglistaler
Abstract:	<p>The weak temperature gradients in the tropical free troposphere due to the vanishing Coriolis force near the equator lead to a strong dynamical coupling over the entire tropics. Using theory and a suite of targeted model experiments, we show that the weak temperature gradients further weaken under global warming. We show that the temperature gradient is set by the circulation strength, with a weaker circulation being associated with weaker gradients. Thus, the known scaling difference between atmospheric radiative cooling and static stability that leads to a slow-down of the circulation under warming also leads to a weakening of the temperature gradients in the tropical free troposphere. The impact from the weakening circulation on the weakening of temperature gradients is shown to dominate over the impact of masked CO₂ forcing and the El-Nino like tropical Pacific warming pattern in model projections. Key to the result is the non-linear zonal momentum advection term. Using the well-known Matsuno-Gill model with correct scaling of heating and static stability may give the correct sign of the response in the temperature gradients, but incorrect scaling, due to the linear momentum damping in that model. The robust scaling of the magnitude of the tropical quasi-stationary structure with temperature opens possibilities for theoretical advances on questions of societal relevance, ranging from changes in tropical cloudiness to heat stress under climate change.</p>
Suggested Reviewers:	Zhiming Kuang kuang@fas.harvard.edu Nicholas Lutsko nlutsko@ucsd.edu Brian Soden bsoden@miami.edu Jiawei Bao jiawei.bao@mpimet.mpg.de John Chiang jch_chiang@berkeley.edu Adam Sobel ahs129@columbia.edu Michael Byrne mpb20@st-andrews.ac.uk

Heng Quan
Program of Atmospheric and Oceanic Sciences,
Department of Geosciences, Princeton University
June 22, 2024

Dear *Journal of the Atmospheric Sciences* Editor:

Enclosed is a manuscript entitled "Weakening of tropical free tropospheric temperature gradients with global warming" that we respectfully submit for consideration for publication in *Journal of the Atmospheric Sciences*. The manuscript is coauthored by Heng Quan, Yi Zhang and Stephan Fueglistaler. Heng Quan will be the corresponding author. The work we present is original and has never been submitted for publication elsewhere. Thank you in advance for your time and consideration.

Sincerely,

Heng Quan
hengquan@princeton.edu



Click here to access/download

Cost Estimation and Agreement Worksheet
Journals Estimation Worksheet New Submission
Format.pdf

1 **Weakening of tropical free tropospheric temperature gradients with global**
2 **warming**

3 Heng Quan,^{a,b} Yi Zhang,^c and Stephan Fueglistaler^{a,b}

4 ^a *Department of Geosciences, Princeton University, Princeton, NJ, US*

5 ^b *Program in Atmospheric and Oceanic Sciences, Princeton University, NJ, US*

6 ^c *Courant Institute of Mathematical Sciences, New York University, NY, US*

7 *Corresponding author: Heng Quan, hengquan@princeton.edu*

8 ABSTRACT: The weak temperature gradients in the tropical free troposphere due to the vanishing
9 Coriolis force near the equator lead to a strong dynamical coupling over the entire tropics. Using
10 theory and a suite of targeted model experiments, we show that the weak temperature gradients
11 further weaken under global warming. We show that the temperature gradient is set by the
12 circulation strength, with a weaker circulation being associated with weaker gradients. Thus, the
13 known scaling difference between atmospheric radiative cooling and static stability that leads to a
14 slow-down of the circulation under warming also leads to a weakening of the temperature gradients
15 in the tropical free troposphere. The impact from the weakening circulation on the weakening of
16 temperature gradients is shown to dominate over the impact of masked CO₂ forcing and the El-Nino
17 like tropical Pacific warming pattern in model projections. Key to the result is the non-linear zonal
18 momentum advection term. Using the well-known Matsuno-Gill model with correct scaling of
19 heating and static stability may give the correct sign of the response in the temperature gradients,
20 but incorrect scaling, due to the linear momentum damping in that model. The robust scaling of
21 the magnitude of the tropical quasi-stationary structure with temperature opens possibilities for
22 theoretical advances on questions of societal relevance, ranging from changes in tropical cloudiness
23 to heat stress under climate change.

24 **1. Introduction**

25 Due to the small Coriolis force at low latitudes, the tropical free troposphere cannot sustain
26 horizontal temperature gradients as large as at higher latitudes (Charney 1963). Any strong
27 horizontal buoyancy or temperature gradients produced by deep convection would be quickly
28 homogenized by gravity waves (Bretherton and Smolarkiewicz 1989). Consequently, on climate
29 time scales horizontal pressure and temperature gradients can be assumed to be small, and the
30 "weak temperature gradient (WTG)" approximation allows to simplify the equations governing the
31 atmospheric dynamics (Sobel and Bretherton 2000; Sobel et al. 2001).

32 The WTG approximation may be used to parameterize tropical planetary-scale circulation in
33 column models (SCMs) and cloud resolving models (CRMs). For example, Sobel and Bretherton
34 (2000) proposed to parameterize the vertical velocity in SCMs in a way that represents the dominant
35 large-scale balance between diabatic heating and vertical advection of potential temperature (Sobel
36 et al. 2001). This approach can be generalized to CRMs (Raymond and Zeng 2005; Sessions
37 et al. 2010; Wang and Sobel 2011; Daleu et al. 2012; Warren et al. 2020); whereby an alternative
38 approach is the "damped gravity wave" method (Kuang 2008; Blossey et al. 2009; Romps 2012;
39 Edman and Romps 2014).

40 Together with the convective quasi-equilibrium (QE) approximation (i.e. moist convection main-
41 tains the vertical temperature profile close to a moist adiabat (Arakawa and Schubert 1974; Emanuel
42 et al. 1994), the QE-WTG framework is the foundation to understand many aspects of tropical cli-
43 mate and changes therein for example due to global warming. In the QE-WTG framework, the
44 tropical troposphere can be seen as consisting of a boundary layer with a substantial tempera-
45 ture gradient and a relatively homogeneous free troposphere whose temperature is determined by
46 the subcloud moist static energy (MSE) in the regions of deep convection where subcloud MSE
47 maximizes (e.g. Emanuel et al. (1994)). This framework has been used to explain the amplified
48 warming over land (Byrne and O’Gorman 2018), an apparent super-moist adiabatic amplification
49 in the tropical temperature trend profile (Flannaghan and Fueglistaler 2014), the trend of tropical
50 heat extremes (Byrne 2021; Zhang et al. 2021), the enhanced precipitation contrast between wet
51 and dry regions with warming (Neelin et al. 2003; Chou and Neelin 2004; Zhang and Fueglistaler
52 2019), and the SST pattern effect and its impact on climate sensitivity (Ceppi and Gregory 2017;
53 Fueglistaler 2019; Fueglistaler and Silvers 2021). Thus, the magnitude of the tropical free tro-

54 tropospheric temperature gradient is of paramount importance for climate, and in the following we
55 address the question how global warming will affect the tropical free tropospheric temperature
56 gradients; specifically, whether the "weak temperature gradient" will get weaker or stronger.

57 The paper is organized as follows. Section 2 provides a brief introduction to the relevant
58 theory and mechanisms. Section 3 describes the numerical models and experiments used in this
59 study. Section 4 discusses the results from model simulations with coupled Atmosphere-Ocean
60 General Circulation Models (GCMs), and Atmospheric GCM simulations with prescribed sea
61 surface temperatures. The simulations show a robust weakening of the temperature gradients
62 independent of the question to what extent global warming results in an El-Nino like warming
63 pattern in the tropics. Similarly, the simulations show that the masked CO₂ forcing is not a
64 major contributor. The weakening of the temperature gradients must result from the slow-down
65 of the atmospheric circulation under global warming, and the zonal momentum equation is used
66 to derive a scaling between temperature gradient and circulation strength. Section 5 shows that
67 idealized mock Walker cell simulations with a CRM follow the theoretical scaling. Finally, Section
68 6 summarizes the results and conclusions, and discusses implications.

69 **2. Theory**

70 *a. Background*

71 The relation between temperature gradients, pressure gradients and the momentum budget is dis-
72 cussed in Charney (1963). However, the impact of the fundamental slow-down of the atmospheric
73 circulation ((Held and Soden 2006)) due to the different scaling of atmospheric radiative cooling
74 and static stability with temperature (the latter being set by the boundary layer specific humidity,
75 which scales approximately like Clausius-Clapeyron) on the quasi-stationary tropical structure of
76 the circulation, pressure and temperature remains incompletely understood.

77 Because of the quasi-stationary geographic structure of atmospheric latent heating in the trop-
78 ics, the tropics show a pronounced quasi-stationary wave structure in the troposphere, whereby
79 temperature gradients maximise in the upper troposphere (warm anomalies in the regions of deep
80 convection) and around the tropical tropopause (cold anomalies over the deep convective regions),
81 with geopotential gradients maximizing in-between (e.g. Fueglistaler (2019)). The model proposed
82 by Gill (1980) provides an elegant approach to understand the tropical tropospheric quasi-stationary

83 structure as the consequence of steady equatorial Rossby and Kelvin waves emanating from the
84 localized heating in the regions of deep convection. The "Gill model" is widely regarded as the
85 basis for any discussion of the large-scale structure of the tropical atmosphere, and would seem the
86 natural starting point for the problem of interest here. However, in order to arrive at an analytical
87 solution, the Gill model represents dissipative processes as linear momentum and diabatic damping
88 (their equations 2.6 - 2.9). The magnitude of the momentum damping coefficient is very important
89 as it sets the length scale of the solution, but the term is physically poorly justified and operates
90 largely as a "tuning" parameter. Our analysis below emphasizes the importance of the momentum
91 balance for the temperature gradient, and the Gill model may not be able to provide the insights
92 necessary to understand the relation between circulation strength and temperature gradient. In
93 passing we note that a superficial look at the Gill solution may suggest an increase in the stationary
94 wave amplitude since the latent heating term Q (precipitation) increases under global warming.
95 The change in static stability with global warming, however, must also be considered, which is
96 - slightly less obvious - encoded in the gravity wave phase speed $c = \frac{NH}{\pi}$ where stratification N
97 is determined by static stability. Because a larger static stability decreases the stationary wave
98 amplitude - which fights against the increase of the latent heating term Q - in a warmer climate, it is
99 not obvious whether the stationary wave amplitude (hence free-tropospheric temperature gradients)
100 will be larger or smaller in a warmer climate just from the Gill model.

101 *b. Expected scaling based on the equatorial zonal momentum balance*

102 The zonal momentum equation at a certain height $z = H$ in the free-troposphere sufficiently far
103 away from the surface is

$$\frac{\partial u}{\partial t} + \mathbf{v} \cdot \nabla u - f v = -\frac{1}{\rho} \frac{\partial p}{\partial x}, \quad (1)$$

104 where u and v are zonal and meridional velocities, \mathbf{v} is the three-dimensional velocity vector, p is
105 pressure, and ρ is air density. The quasi steady-state zonal pressure gradient force in the equatorial
106 upper troposphere is primarily balanced by the zonal advection of zonal momentum (Bao et al.
107 2022)

$$u \frac{\partial u}{\partial x} \approx -\frac{1}{\rho} \frac{\partial p}{\partial x}. \quad (2)$$

108 In the following, we will demonstrate how the left side of Eq. (2) corresponds to the strength of the
 109 overturning circulation W , while the right side is associated with horizontal (virtual) temperature
 110 gradients (δT_v) in the free troposphere, linking δT_v directly to the strength of the atmospheric
 111 circulation.

112 The left side of Eq. (2) corresponds to the overturning circulation strength through mass
 113 conservation

$$\frac{\partial u}{\partial x} + \frac{\partial w}{\partial z} = 0, \quad (3)$$

114 which results in

$$\frac{U}{L} \sim \frac{W}{H}, \quad (4)$$

115 where L is on the scale of 10^4 km, the width of the Equatorial Pacific basin. In addition, the scale
 116 of the zonal variation of u , which we denote as δU in the following, is similar to u itself, i.e.,
 117 $\delta U \sim U$. Therefore, the left side of Eq. (2) scales as

$$\frac{W^2 L}{H^2}. \quad (5)$$

118 The right side of Eq. (2) corresponds to zonal temperature gradients via the hydrostatic balance
 119 and the ideal gas law:

$$\ln \frac{p}{p_s} = -\frac{g}{R_d} \int_0^H \frac{dz}{T_v}, \quad (6)$$

120 where T_v is the height-dependent virtual temperature, and p is the pressure at height $z = H$. In
 121 order to arrive at a scaling, we approximate T_v as constant with height, which is typically valid
 122 when other variables vary more rapidly with height. This simplifies to the hypsometric equation:

$$\ln \frac{p}{p_s} = -\frac{gH}{R_d T_v}. \quad (7)$$

123 Taking the zonal derivative of Eq. (7) and ignoring the zonal variation in p_s , we get

$$\frac{\partial \ln p}{\partial x} = -\frac{gH}{R_d} \frac{\partial}{\partial x} \left(\frac{1}{T_v} \right), \quad (8)$$

124 leading to the scaling

$$\frac{\delta p}{p} \sim \frac{gH\delta T_v}{R_d T_v^2}. \quad (9)$$

125 Combining this with the ideal gas law, the right side of Eq. (2) scales as

$$\frac{gH\delta T_v}{L T_v}. \quad (10)$$

126 We now equate the scalings in Eq. (5) and Eq. (10) and arrive at the following scaling:

$$\frac{\delta T_v}{T_v} \sim \frac{W^2 L^2}{g H^3}. \quad (11)$$

127 This equation links the temperature gradient $\frac{\delta T_v}{T_v}$ to the overturning circulation strength W , hori-
128 zontal length scale L , gravitational acceleration g , and the height of the troposphere H .

129 *c. The importance of the large-scale aggregation of deep convection*

130 The quasi-stationary structure of the tropical atmosphere reflects the large-scale distribution of
131 deep convective heating. Any change in the geographic distribution of deep convection projects on
132 the quasi-stationary structure and hence also on the temperature gradients in the free troposphere.
133 The typical El-Nino like warming pattern over the tropical Pacific leads to an eastward expansion
134 of deep convection, and thus to a weakening of the Walker cell and upper tropospheric temperature
135 gradients over the Pacific. We address the question to what extent the surface warming pattern
136 affects the temperature gradients in the free troposphere with targeted GCM experiments with
137 prescribed SSTs.

138 **3. Methods**

139 *a. General circulation model (GCM) simulations*

140 We use the Geophysical Fluid Dynamics Laboratory (GFDL) Forecast-oriented Low Ocean
141 Resolution version of CM2.5 (CM2.5-FLOR) (Vecchi et al. 2014) and its atmosphere model
142 AM2.5 (Delworth et al. 2012) to conduct patterned and uniform SST warming simulations. The
143 atmosphere and land components of CM2.5-FLOR uses a horizontal resolution of $0.25^\circ \times 0.25^\circ$
144 and 32 vertical levels, and the ocean and sea ice components use lower resolution. The greenhouse

145 gas concentrations except CO₂ and aerosol emissions correspond to the conditions of the year 2000.
146 We run the following experiments:

- 147 1. CM2.5-FLOR idealized CO₂ increase simulation. The CO₂ concentration starts from the
148 observed value at the year 2000 and increases by 1% per year for 140 years (a quadrupling
149 by the year 140). Both CO₂ concentration and SST are changing in this experiment with the
150 coupled Atmosphere Ocean GCM. Averaged fields computed from the first and last 10 years
151 are referred to as “present climate” and “warmer climate”, respectively, and their difference
152 is the response to the CO₂ forcing.
- 153 2. Atmospheric GCM simulations with AM2.5 with prescribed SSTs from the coupled GCM
154 experiment (1) as oceanic boundary condition. The prescribed SSTs are the mean annual
155 cycles of the first and last 10 years of the coupled experiment (1). Both experiments are
156 integrated for 40 years to ensure equilibration, and the last 10 years of both experiments are
157 averaged to obtain the Atmospheric GCM “present climate” and “warmer climate” states. The
158 CO₂ concentration is fixed at the value of the year 2000. These atmospheric GCM climate
159 states allow direct comparison with coupled GCM simulations in (1) and isolate the responses
160 to SST warming under fixed CO₂ forcing, which helps us quantify the masked CO₂ forcing
161 effect (details below).
- 162 3. In order to quantify the importance of the geographic structure of the SST increase in the cou-
163 pled GCM simulations, the atmospheric GCM is run with prescribed SSTs from the “present
164 climate” with a uniform increase corresponding to the global mean SST increase (approx-
165 imately +3 K). The CO₂ concentration is fixed at the value of the year 2000. Comparison of
166 the results with the true (patterned) warming of experiment (2) allows to quantify the impact
167 of the SST warming pattern on the tropical free tropospheric temperature gradients.

168 *b. Cloud resolving model (CRM) simulations*

169 We use the System for Atmospheric Modeling (SAM, Khairoutdinov and Randall (2003)) version
170 6.11.5 cloud resolving model (CRM) for 2-D (longitude/height) mock Walker simulations without
171 rotation similar to Kuang (2012) and Wofsy and Kuang (2012). The model is nonhydrostatic, uses
172 bulk microphysics and a simple Smagorinsky-type scheme for subgrid turbulence, and computes

173 the surface sensible heat, latent heat and momentum fluxes based on the Monin–Obukhov similarity
174 theory. The vertical grid has 64 levels, starting at 25 m and extending up to 27 km, and the vertical
175 grid spacing increases from 50 m at the lowest levels to roughly 1 km at the top of the domain.
176 The model has a rigid lid at the top with a wave-absorbing layer occupying the upper third of
177 the domain to prevent the reflection of gravity waves. The domain width along the x -direction is
178 $L = 10,240$ km with a 2-km horizontal resolution, and solid wall boundary conditions are employed
179 at the two edges.

180 The SSTs are prescribed and linearly decrease by 8 K from the left boundary ($x = 0$) to the right
181 boundary ($x = 10240$ km), mimicking the east-west SST gradient across the equatorial Pacific.
182 Similar to previous studies (Kuang 2012; Wofsy and Kuang 2012), we use prescribed uniform
183 radiative cooling rates Q_{rad} throughout the troposphere (where the temperature is warmer than
184 207.5 K), and use a Newtonian relaxation towards 200 K in the stratosphere (Pauluis and Garner
185 2006). The prescribed radiative cooling allows experiments to disentangle the effects of atmo-
186 spheric humidity on latent heat and static stability, and on the atmospheric radiative cooling. We
187 run two sets of simulations:

- 188 1. Simulations with fixed $Q_{\text{rad}} = -1.7$ K/day and a domain average SST ranging from 294 K to
189 303 K with an increment of +1.5 K (i.e. 7 simulations to cover the range).
- 190 2. Simulations with the domain average SST fixed at 300 K and the radiative cooling Q_{rad} ranging
191 from -2.9 K/day to -0.9 K/day with an increment of 0.2 K/day (i.e. 11 simulations to cover
192 the range).

193 All simulations are run for 150 days and reach equilibrium after approximately 50 days. All our
194 results below show averaged fields computed from the last 50 days of hourly model output.

195 **4. GCM results**

196 Throughout this section, we analyse the virtual temperature $T_v = T(1 + 0.61q)$ (i.e. including
197 the effect of water vapor mixing ratio on density) at the 500 hPa pressure level. We focus on
198 zonal temperature gradients close to equator where the Coriolis force is smallest, and the WTG
199 approximation is most appropriate. The meridional gradients in the GCM simulations are discussed
200 only to the extent necessary for the purpose of this paper. In order to avoid the additional

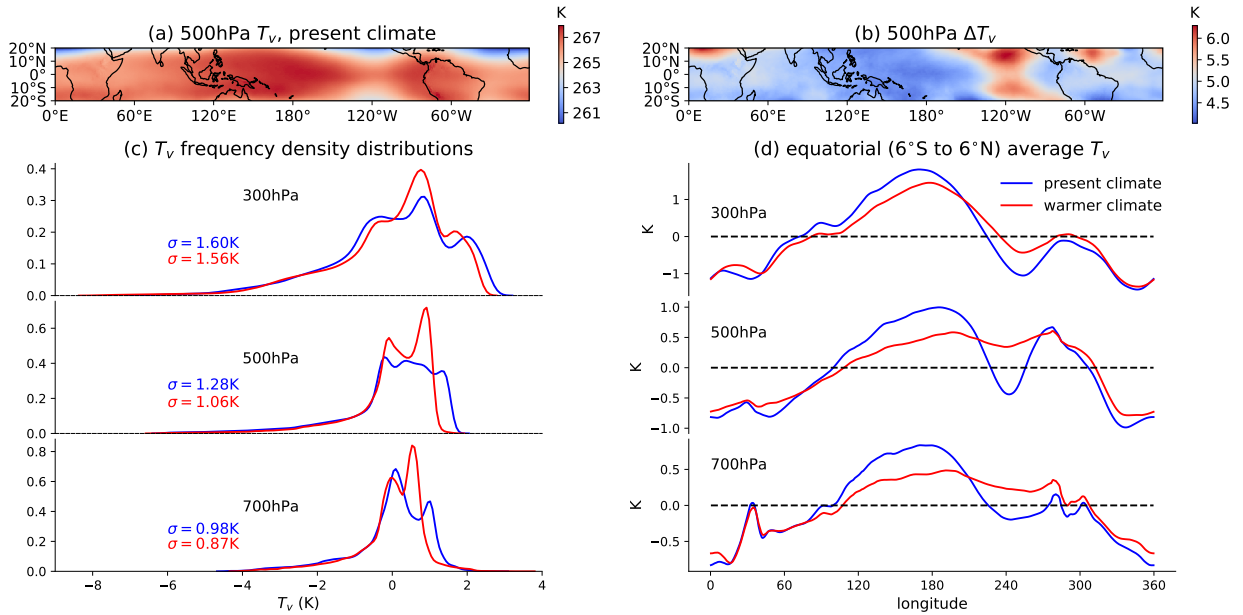
201 complications due to off-equatorial latent heating particularly pronounced during the South Asian
202 monsoon, we focus the following discussion on the results for the month of January; results for the
203 annual mean fields are similar (see Supplement, Figure S2).

204 *a. GCM simulations show weaker temperature gradients in a warmer climate*

205 Figure 1(a) shows that the canonical structure (see also Bao et al. (2022)) of the 500 hPa virtual
206 temperature of the present-climate, with spatial variability of order several Kelvin and temperature
207 maxima over the regions of deep convection (for example, the equatorial Western Pacific warm
208 pool and the Amazon). The global warming simulation retains the geographic structure of the
209 present climate, but the warming structure Figure 1(b,d) reveals an anticorrelation to the anomaly
210 structure of the base state: Regions that are warmer than the average in the base state experience
211 less than average warming, and *vice versa*. Correspondingly, the width (Fig. 1c; quantified in terms
212 of standard deviation) of the frequency distribution of the anomalies from the mean decreases in
213 the "warmer climate" compared to the "present climate" simulation.

214 In the following, we test three possible mechanisms that could explain the decrease in the free
215 tropospheric temperature gradient associated with global warming: Masked CO₂ forcing, changes
216 in the geographic distribution of deep convection due to an El-Nino like SST warming pattern, and
217 the weakening of the tropical diabatic circulation.

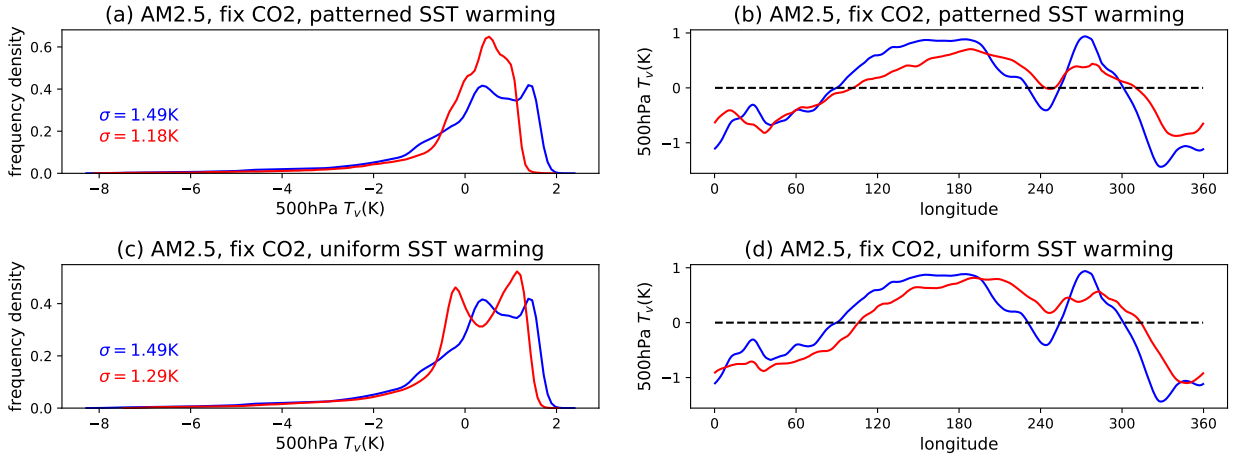
226 **Masked CO₂ forcing.** The first hypothesis is the masked CO₂ forcing. As pointed out by
227 Merlis (2015), although the CO₂ concentration increase is homogeneous over the globe in the
228 global warming simulations, the radiative forcing of CO₂ is not. In the convective regions such
229 as the Western Pacific warm pool, the CO₂ radiative forcing is reduced, or "masked", compared
230 to subsidence regions, by deep-convective clouds and abundant water vapor (see also Zhang and
231 Huang (2014)). Hence, one may hypothesize that this could induce larger free tropospheric warming
232 in the subsiding regions (consistent with the warming pattern visible in Fig. 1(b)). Note that this
233 mechanism is based on the impact on atmospheric radiative cooling, and not inhomogeneous
234 radiative forcing of the surface energy balance. In order to test this hypothesis, We conduct a
235 mechanism-denial model simulation, in which we force AM2.5 (the atmosphere model of CM2.5)
236 with the SST increase from the CM2.5-FLOR CO₂ increase simulation but the CO₂ concentration
237 is fixed at the value of the year 2000 (methods section). This simulation yields, compared to the



218 FIG. 1. Weaker temperature gradients in a warmer climate. (a) January climatological mean 500 hPa virtual
 219 temperature (T_v) in present climate (year 1-10 of the CM2.5-FLOR idealized CO₂ increase simulation). (b)
 220 Response of January climatological mean 500 hPa virtual temperature (ΔT_v) under global warming, calculated
 221 as the difference between warmer climate (year 131-140) and present climate (year 1-10). (c) The frequency
 222 distributions of T_v anomalies from tropical (20°N - 20°S) mean in present climate and warmer climate at 300 hPa,
 223 500 hPa and 700 hPa levels, with their standard deviations σ listed. (d) The zonal profiles of T_v anomalies close
 224 to equator (meridional average between 6°N to 6°S) in present climate and warmer climate at 300 hPa, 500 hPa
 225 and 700 hPa levels.

238 reference simulation with the "masked CO₂ forcing" (Fig. 1), a similar or even stronger weakening
 239 of the temperature gradients in both the frequency distribution (Fig. 2(a)) and the equatorial
 240 meridional mean (Fig. 2(b)).

246 **El-Nino like SST warming.** Coupled GCM simulations yield an El-Nino like warming pattern
 247 over the tropical Pacific in the future (Dong et al. 2019). That is, the cold eastern tropical Pacific
 248 is warming more than the warm western tropical Pacific. This leads to an eastward expansion of
 249 deep convection and a weakening of the Walker cell over the tropical Pacific. Observed SST trends
 250 in recent decades do not show this warming pattern, and there is debate to what extent Walker
 251 cell strength trends are due to the weakening of the diabatic atmospheric circulation (Vecchi et al.
 252 2006) or related to patterned SST warming, and what may cause the difference in the warming



241 FIG. 2. Robust temperature gradient weakening across scenarios. (a) and (b) Same as figure 1 (c) and (d) but
 242 for AM2.5 forced by the patterned SST warming from CM2.5-FLOR idealized CO₂ increase simulation and with
 243 fixed CO₂ concentration. (c) and (d) Same as figure 1 (c) and (d) but for AM2.5 forced by uniform SST warming
 244 resulting the same global mean SST increase as the CM2.5-FLOR idealized CO₂ increase simulation and with
 245 fixed CO₂ concentration. See methods section for simulation details.

253 pattern between coupled GCMs and observations (e.g. Po-Chedley et al. (2021)). The impact of
 254 the El-Nino like warming pattern in coupled GCMs on the Walker cell - and hence also on the
 255 free tropospheric temperature structure (see also Kamae et al. (2015)) - is undisputed, and the
 256 question of interest here is whether this effect dominates, or just contributes, to the weakening of
 257 the temperature gradients shown in Figure 1.

258 In order to quantify the impact of the El-Nino like warming pattern, we conduct a second
 259 mechanism-denial experiment in which we force AM2.5 with a uniform SST increase corresponding
 260 to the global mean SST warming in the CM2.5-FLOR simulation. The results of this simulation
 261 are compared to the simulation with the patterned SST change; both simulations use the same
 262 CO₂ concentration (at the value of the year 2000). This "uniform warming" simulation results
 263 in temperature gradient weakening in both frequency distribution (Fig. 2(c)) and equatorial zonal
 264 profile (Fig. 2(d)), that is smaller, but of comparable magnitude (in terms of reduction of standard
 265 deviation), to the "patterned warming" simulation. Thus, the patterned SST warming trend
 266 amplifies the weakening of the temperature gradients, but is not the dominant reason of weaker
 267 temperature gradients in a warmer climate: The temperature gradients also decrease substantially
 268 under uniform warming.

269 **Slow-down of the circulation.** The weaker scaling of radiative cooling compared to the scaling
 270 of the static stability under global warming implies a a slow-down of the circulation (Held and
 271 Soden 2006; Vecchi and Soden 2007). This slow-down weakens the zonal momentum advection in
 272 the equatorial free troposphere, and a corresponding weakening of the pressure gradient as required
 273 by the zonal momentum balance - which is equivalent to a weaker temperature gradient (Fig. 1d).
 274 Having shown that "masked CO₂" forcing does not lead to, and the patterned warming contributes
 275 but is not the dominant reason for, weaker temperature gradients, we discuss the "circulation
 276 slow-down" mechanism in detail in the next section.

277 *b. Weaker temperature gradients attributed to weaker circulation*

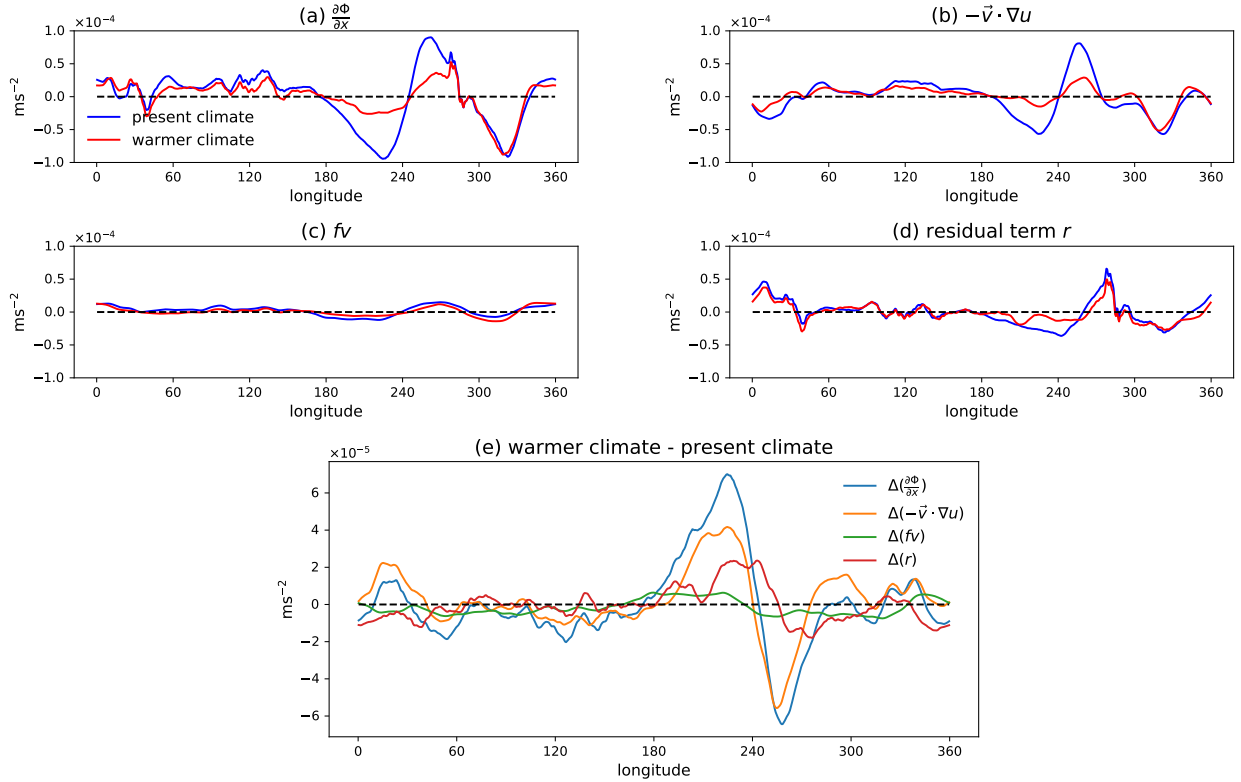
278 To facilitate the analysis of GCM output on pressure levels, we shift to the pressure coordinate
 279 and we focus on geopotential $\Phi = gz$, as Φ and T_v are closely related if we rewrite the hydrostatic
 280 balance (equation 6) in pressure coordinate as

$$\int_{p_s}^p -R_d T_v d \ln p = \int_0^z g dz'. \quad (12)$$

281 That is, the 300 hPa geopotential height z and its response under global warming, Δz , have almost
 282 identical spatial pattern compared to 500 hPa virtual temperature (see Supplement, Figure S1(b,d)).
 283 The temperature gradient weakening in Fig. 1(c)(d) is also reflected in the pressure gradient
 284 weakening in Fig. S1(f)(h). Therefore, we demonstrate that the circulation slow-down decreases
 285 the temperature gradients by showing that the circulation slow-down leads to weaker pressure
 286 gradients due to the steady-state zonal momentum balance:

$$\frac{\partial \Phi}{\partial x} = -\vec{v} \cdot \nabla u + f v + r, \quad (13)$$

287 where the four terms represent pressure gradient force, momentum advection, Coriolis force and
 288 the residual term. As before, we focus on the near-equatorial zonal structure, and show the
 289 10-year January averages of the present and warmer climate coupled GCM simulations. Not
 290 surprisingly, when close to equator, the dominant balance is between the pressure gradient force
 291 and the momentum advection term (i.e. $\frac{\partial \Phi}{\partial x} = -\vec{v} \cdot \nabla u$) in both present climate (first 10 years) and



294 FIG. 3. 300hPa zonal momentum budgets close to equator (meridional average between 6°N to 6°S) for present
 295 (year 1-10) and warmer (year 131-140) climate in the CM2.5-FLOR idealized CO_2 increase simulation. (a)
 296 (minus) Pressure gradient force $\frac{\partial \Phi}{\partial x}$. (b) Zonal momentum advection $-\vec{v} \cdot \nabla u$. (c) Coriolis force $f\bar{v}$. (d) The
 297 residual term r . (e) Responses (difference between warmer climate and present climate) of four terms to global
 298 warming. All terms are January averages in 10 years.

292 warmer climate (last 10 years) (figure 3(a)(b)), while the Coriolis force and the residual term are
 293 relatively small (figure 3(c)(d)).

299 Following global warming, the pressure gradient force and the momentum advection term become
 300 weaker in the equatorial Pacific (Figure 3(a)(b)). The response of the pressure gradient $\Delta\left(\frac{\partial \Phi}{\partial x}\right)$ is
 301 almost equal to the response of the momentum advection $\Delta(-\vec{v} \cdot \nabla u)$ due to the weaker circulation
 302 (Figure 3(e)), with a correlation over all longitudes of 0.91. Consistent with Bao et al. (2022), we
 303 find the reduction of the momentum advection $\Delta(-\vec{v} \cdot \nabla u)$ is dominated by $\Delta\left(-u\frac{\partial u}{\partial x}\right)$ (Supplement,
 304 Figure S4). Therefore, we attribute the weaker 300 hPa zonal pressure gradient as well as the weaker
 305 500 hPa zonal temperature gradient close to equator to weaker momentum advection, which is a

306 consequence of the weaker circulation (primarily weaker Walker circulation in equatorial Pacific)
307 in a warmer climate.

308 Before analysing the relation between circulation strength and temperature gradients more quan-
309 titatively (Section 5), we briefly comment on the weakening of the meridional temperature and
310 pressure gradients, which is particularly prominent over the subtropical Eastern Pacific and North
311 Africa (Fig. 1(b)). In these regions, the Coriolis force is no longer negligible, and the reduction of
312 the pressure gradient force $\Delta\left(-\frac{\partial\Phi}{\partial y}\right)$ in response to global warming is balanced by the reduction of
313 the Coriolis force $\Delta(-fu)$ (figure S3), itself a consequence of weaker westerly wind. Future work
314 may focus on this result, and its relation to the discussion of the response of the subtropical jet to
315 global warming (Rivière 2011; Woollings et al. 2023).

316 5. Theoretical scalings and CRM results

317 In the following, we seek theoretical understanding using a simple model, aligned with the
318 hierarchical approach (Held 2005). As mentioned before, the linear Matsuno-Gill model would
319 be an obvious starting point due to its ability to reproduce the spatial pattern of 500 hPa ΔT_v .
320 By converting the predicted change of convective heating (i.e. precipitation) to the forcing Q
321 in the Gill model thermal equation (equation 2.8 in Gill (1980)), the tropical free troposphere
322 temperature gradients are weaker in a warmer climate ¹ (Keil et al. (2023), their Figure 5).
323 However, the linear Matsuno-Gill model cannot give the correct explanation. According to the
324 zonal momentum equation (equation 2.6 in Gill (1980)) in the Matsuno-Gill model, one would
325 attribute a weaker pressure gradient $-\frac{\partial p}{\partial x}$ along the equator to a weaker momentum damping that
326 is *linearly* proportional to the zonal wind, i.e. $-\epsilon \cdot u$. Below, we show that numerical model
327 simulations do not follow the linear scaling inherent in the Matsuno-Gill model, but follow the
328 (quadratic) scaling derived in Section 2.

329 Hence, we turn to a 2-dimensional (longitude/height) numerical model simulation in order to
330 evaluate the theoretical scaling (Section 2, eq. 11) based on the zonal momentum equation with
331 the dominant term $-\vec{v} \cdot \nabla u$. In these 2-D mock Walker cell simulations deep convection gradually
332 becomes weaker away from the warm end, and is absent in the colder part of the domain.

¹Note: Keil et al. (2023) did not adjust gravity wave phase speed (i.e. stratification) in the Gill model, which increases under global warming. Therefore, their results cannot be regarded as a "global warming" calculation.

333 The numerical experiments employ uniform radiative cooling rates Q_{rad} throughout the tropo-
 334 sphere and linear SST profiles as shown in Fig. 4(a). This configuration is similar to the real-world
 335 equatorial Pacific and forces the majority of deep convection (and precipitation) to develop in
 336 the leftmost (warmest) 20% of the domain (Fig. 4(a)), resulting in a mock Walker circulation
 337 (Fig. 4(b)). The circulation strength is controlled by variation of the radiative cooling rate. In the
 338 limit where the steady-state thermodynamic energy equation is dominated by a balance of radiative
 339 cooling and vertical motion (typical in subsidence regions above cold SSTs), we can relate the
 340 strength of the vertical motion required by the scaling to the prescribed radiative cooling as

$$w = \frac{Q_{\text{rad}}}{S} = \frac{Q_{\text{rad}}}{\frac{\partial T}{\partial z} + \frac{g}{c_p}}, \quad (14)$$

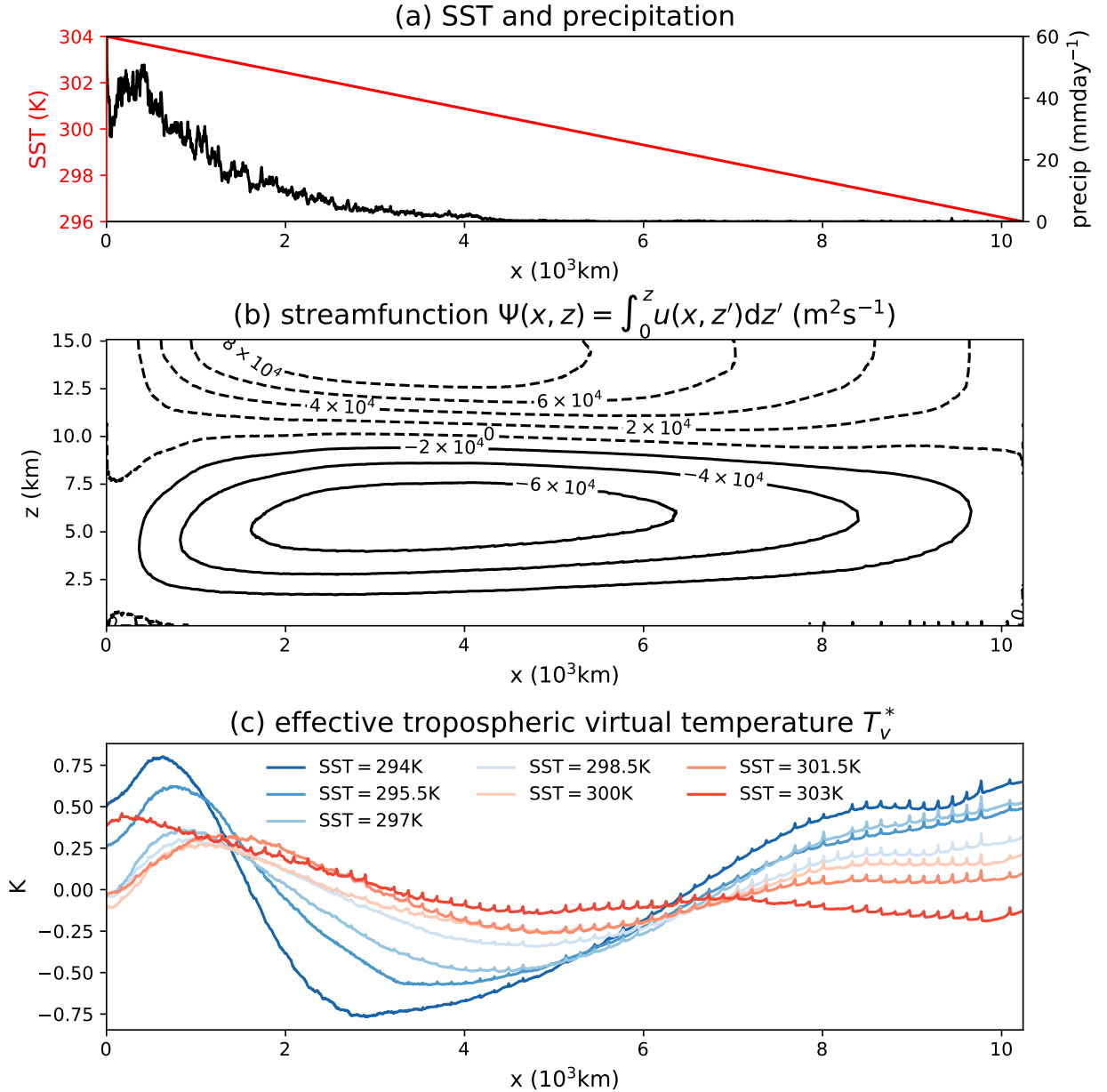
341 where $Q_{\text{rad}} < 0$ is the radiative cooling rate in K s^{-1} and $S = \frac{\partial T}{\partial z} + \frac{g}{c_p}$ is the dry stability in K m^{-1} .

346 Equation 14 shows that, in addition to variations of the radiative cooling rate, the circulation
 347 strength can also be modified by variations in the static stability. As mentioned before, under
 348 global warming both parameters change, and the net slow down results from the static stability
 349 scaling being larger than the radiative cooling scaling with warming. Hence, we run two sets of
 350 experiments:

- 351 1. Variation of the domain average SST from 294 K to 303 K with a step of 1.5 K., while fixing
 352 the radiative cooling rate Q_{rad} at -1.7 K/day. Higher SSTs lead to higher subcloud specific
 353 humidity, which increases the static stability S . Hence, at fixed radiative cooling the simulation
 354 with higher SSTs is expected to show a weaker circulation (see also Appendix A, Figure A1).
- 355 2. Variation of the radiative cooling rate Q_{rad} from -2.9 K/day to -0.9 K/day with a step of
 356 0.2 K/day, while fixing the domain average SST at 300 K to fix stability S . At fixed SSTs
 357 and hence fixed S , the simulation with a smaller radiative cooling rate is expected to show a
 358 weaker circulation (see also Appendix A, Figure A2).

359 From the hydrostatic equation 6, we define an effective tropospheric virtual temperature T_v^* to
 360 represent the free troposphere temperature as:

$$T_v^* = -\frac{gH}{R_d \ln \frac{p}{p_s}}, \quad (15)$$



342 FIG. 4. (a) SST and precipitation profiles and (b) the overturning streamfunction for the simulation with
 343 $Q_{\text{rad}} = -2.1$ K/day and mean SST of 300 K. (c) The effective tropospheric virtual temperature T_v^* (details in
 344 text) anomalies (from averages along x direction) in SAM simulations with fixed radiative cooling rate $Q_{\text{rad}} =$
 345 -1.7 K/day but different mean SSTs.

361 which is the virtual temperature of an isothermal atmosphere with the same pressure-height relation
 362 at pressure p (in the upper troposphere) as the (not isothermal) atmosphere in the numerical model
 363 simulation.

364 For the simulations with varying radiative cooling but equal SSTs, the equivalent virtual temper-
 365 ature is evaluated for $H = 10$ km. For the simulations with varying SSTs but equal radiative cooling,
 366 the height level is determined as the level where the (horizontal) average temperature $\langle T \rangle = 220$ K.
 367 See Appendix A for motivation and further details. Actual virtual temperature at different levels
 368 from the $z = 5$ km level to the $z = 10$ km level show similar results as the effective tropospheric
 369 virtual temperature T_v^* (Supplement, Figure S6). Hence, the effective virtual temperature is a
 370 convenient and accurate parameter.

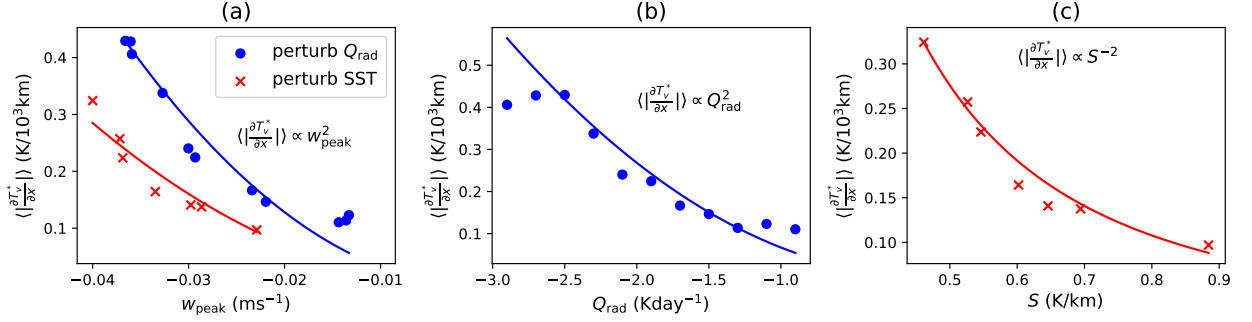
371 Figure 4(c) shows that, as expected, the simulations with higher SSTs have a weaker circulation,
 372 and a weaker temperature gradient in the free troposphere (i.e. a flatter T_v^* profile). Similarly
 373 (not shown), the simulations with equal SSTs but varying radiative cooling rate show a weaker
 374 circulation and a flatter T_v^* profile for the simulations with smaller radiative cooling. Qualitatively,
 375 the 2-D CRM results are consistent with the GCM results and confirm that a weaker circulation is
 376 associated with weaker temperature gradients in free troposphere. Thus, the idealized mock Walker
 377 cell simulations can be used to quantitatively evaluate the scaling between circulation strength and
 378 temperature gradients.

379 The horizontal temperature gradient is expected to scale with the square of subsiding velocity
 380 (W^2) all else held fixed (Equation 11). Replacing W in equation 11 with the peak subsiding velocity
 381 w_{peak} in the subsiding branch (details in appendix A) gives

$$\langle \left| \frac{\partial T_v^*}{\partial x} \right| \rangle \propto w_{\text{peak}}^2, \quad (16)$$

382 where $\langle \left| \frac{\partial T_v^*}{\partial x} \right| \rangle$ is the average (absolute) horizontal T_v^* (eq. 15) gradient along the x-direction. The
 383 proportionality coefficient in equation 16 is given by equation B8 in the Appendix B.

384 Figure 5(a) shows that the theoretical relation in equation 16 (curves) is consistent with the model
 385 results (dots), both when we change Q_{rad} with fixed SST (blue) and change SST with fixed Q_{rad} (red).
 386 Consistent with equation 14, Figure 5(b) shows that $\langle \left| \frac{\partial T_v^*}{\partial x} \right| \rangle \propto Q_{\text{rad}}^2$ when varying Q_{rad} with fixed
 387 SST, and Figure 5(c) shows that $\langle \left| \frac{\partial T_v^*}{\partial x} \right| \rangle \propto S^{-2}$ when varying SSTs with fixed Q_{rad} . Therefore, the
 388 mock Walker cell numerical model simulations quantitatively confirm that the weaker circulation
 389 causes weaker temperature gradients in tropical free troposphere, and that the temperature gradient
 390 scales with the *square* of circulation strength (i.e. w_{peak}^2). Using the linear Matsuno-Gill model
 391 (e.g. Keil et al. (2023)) to analyse the relation between circulation and temperature gradients, and



395 FIG. 5. Weaker circulation causes weaker temperature gradients in CRM simulations. (a) The average
 396 (absolute) horizontal T_v^* (defined in equation 15) gradient along x direction, $\langle |\frac{\partial T_v^*}{\partial x}| \rangle$, as a function of the peak
 397 subsiding velocity w_{peak} in the subsiding branch (details in appendix A) when we change Q_{rad} under fixed SST
 398 (blue) and change SST under fixed Q_{rad} (red). The dots are model results, and the curves are parabolas going
 399 through the origin (equation B8 in appendix B). (b) Same as (a) but showing $\langle |\frac{\partial T_v^*}{\partial x}| \rangle$ as a function of Q_{rad} when
 400 we change Q_{rad} under fixed SST. (c) Same as (a) but showing $\langle |\frac{\partial T_v^*}{\partial x}| \rangle$ as a function of stability S when we change
 401 SST under fixed Q_{rad} .

392 how it may change under global warming, gives the incorrect result that the temperature (pressure)
 393 gradient scales *linearly* with circulation strength (i.e. U or W) because the pressure gradient force
 394 $-\frac{1}{\rho} \frac{\partial p}{\partial x}$ is balanced by the linear momentum damping term $-au$ (equation 2.6 in Gill (1980)).

402 Finally, we note that the $\langle |\frac{\partial T_v^*}{\partial x}| \rangle \propto w_{\text{peak}}^2$ theory seems to hold only for a certain range of the
 403 circulation strength. Figure 5(b) shows that when the radiative cooling is smaller (in magnitude)
 404 than -1.5 K/day or larger (in magnitude) than -2.5 K/day , the scaling is no longer accurate.
 405 Inspection of the circulation structure (Supplement, Figure S7) shows that the simulations show a
 406 regime shift, changing from a single cell to a double cell when Q_{rad} becomes smaller (in magnitude)
 407 than -1.5 K/day . This regime shift has also been noted in similar situations by Lutsko and Cronin
 408 (2023). The scaling and its evaluation at a height of $\approx 10 \text{ km}$ applies to the situation of a single
 409 overturning cell with 10 km being robustly in the upper troposphere (see Appendix B). The cause
 410 for the regime shift, and adapting the scaling and its evaluation to multiple cells, are beyond the
 411 scope here, but are important questions for future research.

412 **6. Conclusions and outlook**

413 Due to the smallness of the Coriolis parameter at low latitudes, the tropical free troposphere
414 cannot maintain temperature gradients as large as at higher latitudes (Charney 1963). Using theory
415 and a hierarchy of models, we demonstrate that horizontal temperature gradients in the tropical free
416 troposphere will be even weaker in a warmer climate. This is because the magnitude of the temper-
417 ature gradients scale with the circulation strength, and the circulation strength decreases with global
418 warming (Held and Soden 2006; Vecchi and Soden 2007). The weaker circulation corresponds to
419 weaker horizontal momentum advection, which then causes weaker horizontal pressure gradients
420 in the tropical free troposphere as required by the steady-state zonal momentum equation. Due
421 to hydrostatic balance, the weaker pressure gradients correspond to weaker temperature gradients.
422 This theoretical expectations is confirmed by the GCM simulations and quantitatively verified by
423 the CRM mock Walker circulation simulations shown in this paper.

424 Linear models, such as the Matsuno-Gill model forced by predicted change of convective heating
425 (i.e. precipitation) and stratification also yield a weakening of the temperature gradient in the free
426 troposphere due to the weakening of the circulation. However, the scaling would not be correct
427 as the Matsuno-Gill model employs a linear momentum damping, whereas in reality the zonal
428 momentum equation is quadratic. The 2-D mock Walker circulation model simulations shown
429 here confirm the quadratic scaling.

430 Our results have implications for both idealized modeling and theoretical understanding of the
431 tropical atmosphere. Parameterizations of large-scale dynamics in SCMs and CRMs need to
432 correctly represent the weakening of temperature gradient in simulations of global warming. Our
433 results highlight the importance of the non-linear momentum advection term for the understanding
434 of changes in atmospheric dynamics with global warming and climate change in general. Direct
435 implications of the weakening of the temperature gradient in tropical free troposphere include
436 processes that depend on the static stability of the lower troposphere, including heat extremes
437 (Sherwood and Huber 2010; Zhang et al. 2021) and low cloud amount (Klein and Hartmann 1993;
438 Ceppi and Gregory 2017; Fueglistaler 2019).

439 *Acknowledgments.* Heng Quan thanks Timothy Merlis, Zhihong Tan and Gabriel Vecchi for
440 helpful discussions. Heng Quan thanks Andrew Williams for guidance on running cloud resolving
441 simulations. Heng Quan thanks Wenchang Yang for providing the CM2.5 global warming simu-

442 lation results. Computations in this research are done on the Tiger cluster and Stellar cluster of
443 Princeton University.

444 *Data availability statement.* The model outputs and data used in this study are available upon
445 request.

446 APPENDIX A

447 **Two ways to vary the strength of the mock Walker circulation**

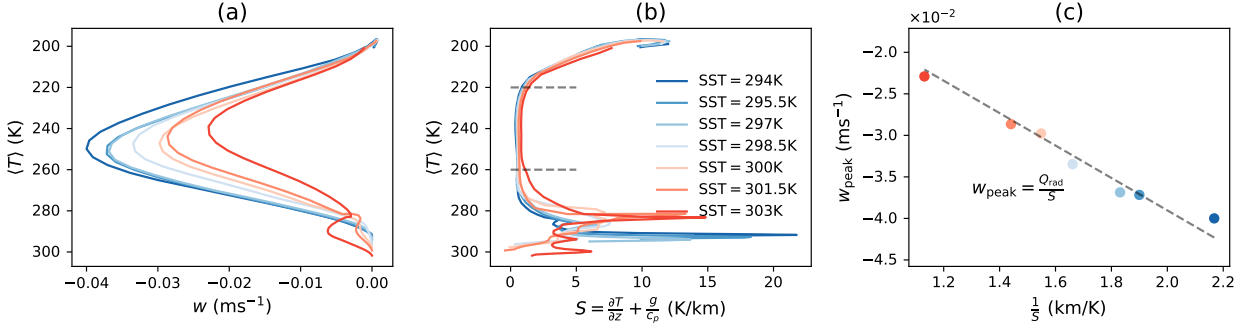
448 The circulation strength (i.e. subsidence velocity) may be modified (eqn. 14) by either changing
449 SSTs (to change static stability S) or by changing the radiative cooling rate Q_{rad} .

450 When increasing SSTs under fixed Q_{rad} , the subsiding velocity w indeed becomes smaller
451 (Figure A1a). This is because the stability $S = \frac{\partial T}{\partial z} + \frac{g}{c_p}$ in the free troposphere (vertically averaged
452 between the $\langle T \rangle = 260$ K level and the $\langle T \rangle = 220$ K level) becomes larger in Fig. A1(b). The
453 theoretical relation $w_{\text{peak}} = \frac{Q_{\text{rad}}}{S}$ (line) is consistent with the model results (dots) in Fig. A1(c). Note
454 that in Figure A1(a)(b) we follow Jeevanjee (2022) and use temperature as the vertical coordinate.
455 This is because the circulation structure (i.e. w in figure A1(a)) remains approximately fixed in
456 temperature coordinates, so this choice simplifies our analysis when warmer SST deepens the
457 troposphere.

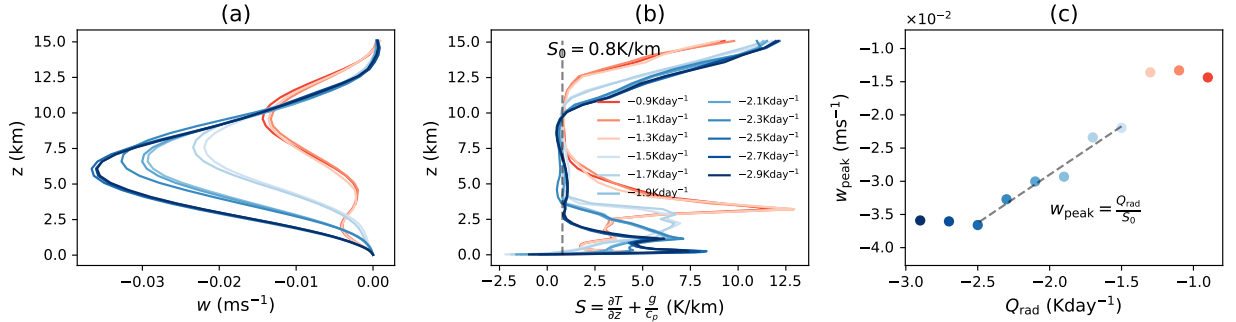
464 Decreasing Q_{rad} under fixed SST, the subsiding velocity w becomes smaller (Figure A2a). In this
465 experiment, the stability $S = \frac{\partial T}{\partial z} + \frac{g}{c_p}$ near the peak subsiding velocity in Fig. A2(b) has a constant
466 value $S_0 \approx 0.8$ K/km for different radiative cooling rates. The theoretical relation $w_{\text{peak}} = \frac{Q_{\text{rad}}}{S_0}$
467 (line) is consistent with model results (dots) in Fig. A2(c) when Q_{rad} is between -2.5 K/day and
468 -1.5 K/day. When Q_{rad} is smaller (in magnitude) than -1.5 K/day or larger (in magnitude) than
469 -2.5 K/day, however, the subsiding velocity departs from the expected scaling with the radiative
470 cooling rate. Inspection of the mass stream function shows that there is a regime shift (figure S7)
471 where equation (14) is no longer accurate.

478 APPENDIX B

479 **The theoretical relation between temperature gradient and subsiding velocity**



458 FIG. A1. Tropospheric vertical profiles of (a) vertical velocity w and (b) stability $S = \frac{\partial T}{\partial z} + \frac{g}{c_p}$ in the subsiding
 459 branch (i.e. average along x direction above the 10% coldest SSTs) of SAM simulations with the same radiative
 460 cooling rate $Q_{\text{rad}} = -1.7$ K/day but different mean SSTs. Notice here we use temperature as the vertical coordinate.
 461 (c) The peak subsiding velocity w_{peak} as a function of $\frac{1}{S}$, where S is averaged between the two dotted lines in (b) -
 462 the $\langle T \rangle = 260$ K level and the $\langle T \rangle = 220$ K level. The dotted line in (c) shows their predicted relation $w_{\text{peak}} = \frac{Q_{\text{rad}}}{S}$
 463 based on theory (details in text).



472 FIG. A2. Tropospheric vertical profiles of (a) vertical velocity w and (b) stability $S = \frac{\partial T}{\partial z} + \frac{g}{c_p}$ in the subsiding
 473 branch (i.e. average along x direction above the 20% coldest SSTs) of SAM simulations with the same mean
 474 SST of 300 K but different radiative cooling rates Q_{rad} . (c) The peak subsiding velocity w_{peak} as a function of the
 475 radiative cooling rate Q_{rad} . The dotted line shows their predicted relation $w_{\text{peak}} = \frac{Q_{\text{rad}}}{S_0}$ based on theory (details
 476 in text), where $S_0 \approx 0.8$ K/km is the constant stability in mid-troposphere for different radiative cooling rates as
 477 marked in (b).

480 First, we derive how u scales with w from the continuity equation. We assume that the subsiding
 481 vertical velocity w close to the cold end of the domain $x = L$ (Fig.A1(a) and Fig.A2(a)) has the
 482 highly idealized form of

$$w = w_{\text{peak}} \sin \frac{\pi z}{H}, \quad (\text{B1})$$

483 where $H = 10\text{km}$ when we change Q_{rad} under fixed SST and H is the level where $\langle T \rangle = 220\text{ K}$
 484 when we change SST under fixed Q_{rad} . We also assume the horizontal velocity u at the $z = H$ level
 485 (figure not shown) has the highly idealized form of

$$u = u_{\text{peak}} \sin \frac{\pi x}{L}, \quad (\text{B2})$$

486 where the domain width $L = 10240\text{ km}$. Evaluating the continuity equation 3 at $(x, z) = (L, H)$
 487 gives

$$u_{\text{peak}} = -\frac{L}{H} w_{\text{peak}}. \quad (\text{B3})$$

488 The functional forms of this idealization are applicable only to cells with length scales L and H ;
 489 the regime shift to double cells violates this idealization.

490 Second, we derive how pressure gradient scales with w from the momentum equation. Hourly
 491 CRM output enables us to decompose the momentum advection terms into stationary terms and
 492 eddy terms, and rewrite the momentum equation (13) as (Yang et al. 2013)

$$-\frac{\overline{1}}{\rho} \frac{\partial p}{\partial x} + \left(-\overline{u} \frac{\partial \overline{u}}{\partial x} \right) + \left(-\overline{w} \frac{\partial \overline{u}}{\partial z} \right) + \left(-\frac{\partial \overline{u'u'}}{\partial x} \right) + \left(-\frac{\partial \overline{u'w'}}{\partial z} \right) + \overline{r} = 0, \quad (\text{B4})$$

493 where $\overline{(\)}$ is the time average. The six terms in this equation are plotted in the Supplement
 494 Figure S5 (a) to (f) for the simulation with $Q_{\text{rad}} = -2.1\text{ K/day}$ and mean SST of 300 K . At the
 495 $z = H$ level in free troposphere, the dominant balance is between the pressure gradient force and
 496 the stationary horizontal advection of horizontal momentum (figure S5(g)), so we assume

$$-\frac{\overline{1}}{\rho} \frac{\partial p}{\partial x} + \left(-\overline{u} \frac{\partial \overline{u}}{\partial x} \right) = 0. \quad (\text{B5})$$

497 Utilizing equation (B2) for u and neglecting density variation, the pressure gradient has the form

$$\frac{\partial p}{\partial x} = -\rho u_{\text{peak}}^2 \frac{\pi}{2L} \sin \frac{2\pi x}{L}, \quad (\text{B6})$$

498 so that the average (absolute) horizontal pressure gradient along the x-direction is

$$\langle |\frac{\partial p}{\partial x}| \rangle = \frac{\rho}{L} u_{\text{peak}}^2 = \frac{\rho L}{H^2} w_{\text{peak}}^2. \quad (\text{B7})$$

499 Finally, we derive the temperature gradient scaling with w from the hydrostatic equation. We
500 compute the x-derivative of the effective tropospheric virtual temperature T_v^* defined in equation
501 15. Neglecting the horizontal variation of p_s (we would get an additional constant term because
502 p_s gradient is tied to SST gradient and approximately fixed), we can relate $\langle |\frac{\partial T_v^*}{\partial x}| \rangle$ to $\langle |\frac{\partial p}{\partial x}| \rangle$ by

$$\langle |\frac{\partial T_v^*}{\partial x}| \rangle = \frac{gH}{R_d} \frac{1}{p \cdot (\ln p/p_s)^2} \langle |\frac{\partial p}{\partial x}| \rangle = \frac{g}{R_d} \frac{1}{p \cdot (\ln p/p_s)^2} \frac{\rho L}{H} w_{\text{peak}}^2. \quad (\text{B8})$$

503 This equation tells us the coefficient in equation 16. Using $w_{\text{peak}} = \frac{Q_{\text{rad}}}{S}$, we can also get the
504 coefficients for $\langle |\frac{\partial T_v^*}{\partial x}| \rangle \propto Q_{\text{rad}}^2$ and $\langle |\frac{\partial T_v^*}{\partial x}| \rangle \propto S^{-2}$. Figure 5 shows that the theoretical relations
505 derived here (curves) are consistent with model results (dots).

506 **References**

- 507 Arakawa, A., and W. H. Schubert, 1974: Interaction of a cumulus cloud ensemble with the
508 large-scale environment, part I. *Journal of the atmospheric sciences*, **31 (3)**, 674–701.
- 509 Bao, J., V. Dixit, and S. C. Sherwood, 2022: Zonal temperature gradients in the tropical free
510 troposphere. *Journal of Climate*, **35 (24)**, 4337–4348.
- 511 Blossey, P. N., C. S. Bretherton, and M. C. Wyant, 2009: Subtropical low cloud response to a
512 warmer climate in a superparameterized climate model. Part II: Column modeling with a cloud
513 resolving model. *Journal of Advances in Modeling Earth Systems*, **1 (3)**.
- 514 Bretherton, C. S., and P. K. Smolarkiewicz, 1989: Gravity waves, compensating subsidence and
515 detrainment around cumulus clouds. *Journal of Atmospheric Sciences*, **46 (6)**, 740–759.
- 516 Byrne, M. P., 2021: Amplified warming of extreme temperatures over tropical land. *Nature*
517 *Geoscience*, **14 (11)**, 837–841.
- 518 Byrne, M. P., and P. A. O’Gorman, 2018: Trends in continental temperature and humidity directly
519 linked to ocean warming. *Proceedings of the National Academy of Sciences*, **115 (19)**, 4863–
520 4868.
- 521 Ceppi, P., and J. M. Gregory, 2017: Relationship of tropospheric stability to climate sensitivity and
522 Earth’s observed radiation budget. *Proceedings of the National Academy of Sciences*, **114 (50)**,
523 13 126–13 131.
- 524 Charney, J. G., 1963: A note on large-scale motions in the tropics. *Journal of the Atmospheric*
525 *Sciences*, **20 (6)**, 607–609.
- 526 Chou, C., and J. D. Neelin, 2004: Mechanisms of global warming impacts on regional tropical
527 precipitation. *Journal of climate*, **17 (13)**, 2688–2701.
- 528 Daleu, C. L., S. J. Woolnough, and R. Plant, 2012: Cloud-resolving model simulations with
529 one-and two-way couplings via the weak temperature gradient approximation. *Journal of the*
530 *Atmospheric Sciences*, **69 (12)**, 3683–3699.
- 531 Delworth, T. L., and Coauthors, 2012: Simulated climate and climate change in the GFDL CM2.5
532 high-resolution coupled climate model. *Journal of Climate*, **25 (8)**, 2755–2781.

533 Dong, Y., C. Proistosescu, K. C. Armour, and D. S. Battisti, 2019: Attributing historical and future
534 evolution of radiative feedbacks to regional warming patterns using a Green's function approach:
535 The preeminence of the western Pacific. *Journal of Climate*, **32** (17), 5471–5491.

536 Edman, J. P., and D. M. Romps, 2014: An improved weak pressure gradient scheme for single-
537 column modeling. *Journal of the Atmospheric Sciences*, **71** (7), 2415–2429.

538 Emanuel, K. A., J. David Neelin, and C. S. Bretherton, 1994: On large-scale circulations in
539 convecting atmospheres. *Quarterly Journal of the Royal Meteorological Society*, **120** (519),
540 1111–1143.

541 Flannaghan, T. J., and S. Fueglistaler, 2014: Vertical mixing and the temperature and wind structure
542 of the tropical tropopause layer. *Journal of the Atmospheric Sciences*, **71** (5), 1609–1622.

543 Fueglistaler, S., 2019: Observational evidence for two modes of coupling between sea surface
544 temperatures, tropospheric temperature profile, and shortwave cloud radiative effect in the
545 tropics. *Geophysical Research Letters*, **46** (16), 9890–9898.

546 Fueglistaler, S., and L. Silvers, 2021: The peculiar trajectory of global warming. *Journal of*
547 *Geophysical Research: Atmospheres*, **126** (4), e2020JD033 629.

548 Gill, A. E., 1980: Some simple solutions for heat-induced tropical circulation. *Quarterly Journal*
549 *of the Royal Meteorological Society*, **106** (449), 447–462.

550 Held, I. M., 2005: The gap between simulation and understanding in climate modeling. *Bulletin*
551 *of the American Meteorological Society*, **86** (11), 1609–1614.

552 Held, I. M., and B. J. Soden, 2006: Robust responses of the hydrological cycle to global warming.
553 *Journal of climate*, **19** (21), 5686–5699.

554 Jeevanjee, N., 2022: Three rules for the decrease of tropical convection with global warming.
555 *Journal of Advances in Modeling Earth Systems*, **14** (11), e2022MS003 285.

556 Kamae, Y., H. Shiogama, M. Watanabe, M. Ishii, H. Ueda, and M. Kimoto, 2015: Recent slowdown
557 of tropical upper tropospheric warming associated with Pacific climate variability. *Geophysical*
558 *Research Letters*, **42** (8), 2995–3003.

559 Keil, P., H. Schmidt, B. Stevens, M. Byrne, H. Segura, and D. Putrasahan, 2023: Tropical
560 tropospheric warming pattern explained by shifts in convective heating in the Matsuno–Gill
561 model. *Quarterly Journal of the Royal Meteorological Society*, **149 (756)**, 2678–2695.

562 Khairoutdinov, M. F., and D. A. Randall, 2003: Cloud resolving modeling of the ARM summer
563 1997 IOP: Model formulation, results, uncertainties, and sensitivities. *Journal of the Atmospheric
564 Sciences*, **60 (4)**, 607–625.

565 Klein, S. A., and D. L. Hartmann, 1993: The seasonal cycle of low stratiform clouds. *Journal of
566 Climate*, **6 (8)**, 1587–1606.

567 Kuang, Z., 2008: Modeling the interaction between cumulus convection and linear gravity waves
568 using a limited-domain cloud system–resolving model. *Journal of the Atmospheric Sciences*,
569 **65 (2)**, 576–591.

570 Kuang, Z., 2012: Weakly forced mock Walker cells. *Journal of the Atmospheric Sciences*, **69 (9)**,
571 2759–2786.

572 Lutsko, N., and T. W. Cronin, 2023: Mock-walker simulations: Mean climates, responses to
573 warming and transition to double-cell circulations. *Authorea Preprints*.

574 Merlis, T. M., 2015: Direct weakening of tropical circulations from masked CO₂ radiative forcing.
575 *Proceedings of the National Academy of Sciences*, **112 (43)**, 13 167–13 171.

576 Neelin, J., C. Chou, and H. Su, 2003: Tropical drought regions in global warming and El Niño
577 teleconnections. *Geophysical Research Letters*, **30 (24)**.

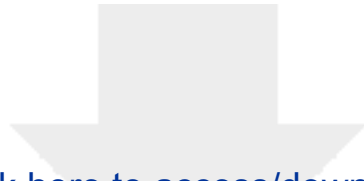
578 Pauluis, O., and S. Garner, 2006: Sensitivity of radiative-convective equilibrium simulations to
579 horizontal resolution. *Journal of the atmospheric sciences*, **63 (7)**, 1910–1923.

580 Po-Chedley, S., B. D. Santer, S. Fueglistaler, M. D. Zelinka, P. J. Cameron-Smith, J. F. Painter,
581 and Q. Fu, 2021: Natural variability contributes to model–satellite differences in tropical tropo-
582 spheric warming. *Proceedings of the National Academy of Sciences*, **118 (13)**, e2020962 118.

583 Raymond, D. J., and X. Zeng, 2005: Modelling tropical atmospheric convection in the context of
584 the weak temperature gradient approximation. *Quarterly Journal of the Royal Meteorological*

- 585 *Society: A journal of the atmospheric sciences, applied meteorology and physical oceanography*,
586 **131 (608)**, 1301–1320.
- 587 Rivière, G., 2011: A dynamical interpretation of the poleward shift of the jet streams in global
588 warming scenarios. *Journal of the Atmospheric Sciences*, **68 (6)**, 1253–1272.
- 589 Romps, D. M., 2012: Weak pressure gradient approximation and its analytical solutions. *Journal*
590 *of the atmospheric sciences*, **69 (9)**, 2835–2845.
- 591 Sessions, S. L., S. Sugaya, D. J. Raymond, and A. H. Sobel, 2010: Multiple equilibria in a cloud-
592 resolving model using the weak temperature gradient approximation. *Journal of Geophysical*
593 *Research: Atmospheres*, **115 (D12)**.
- 594 Sherwood, S. C., and M. Huber, 2010: An adaptability limit to climate change due to heat stress.
595 *Proceedings of the National Academy of Sciences*, **107 (21)**, 9552–9555.
- 596 Sobel, A. H., and C. S. Bretherton, 2000: Modeling tropical precipitation in a single column.
597 *Journal of climate*, **13 (24)**, 4378–4392.
- 598 Sobel, A. H., J. Nilsson, and L. M. Polvani, 2001: The weak temperature gradient approximation
599 and balanced tropical moisture waves. *Journal of the atmospheric sciences*, **58 (23)**, 3650–3665.
- 600 Vecchi, G. A., and B. J. Soden, 2007: Global warming and the weakening of the tropical circulation.
601 *Journal of Climate*, **20 (17)**, 4316–4340.
- 602 Vecchi, G. A., B. J. Soden, A. T. Wittenberg, I. M. Held, A. Leetmaa, and M. J. Harrison, 2006:
603 Weakening of tropical pacific atmospheric circulation due to anthropogenic forcing. *Nature*,
604 **441 (7089)**, 73–76.
- 605 Vecchi, G. A., and Coauthors, 2014: On the seasonal forecasting of regional tropical cyclone
606 activity. *Journal of Climate*, **27 (21)**, 7994–8016.
- 607 Wang, S., and A. H. Sobel, 2011: Response of convection to relative sea surface temperature:
608 Cloud-resolving simulations in two and three dimensions. *Journal of Geophysical Research:*
609 *Atmospheres*, **116 (D11)**.
- 610 Warren, R. A., M. S. Singh, and C. Jakob, 2020: Simulations of radiative-convective-dynamical
611 equilibrium. *Journal of Advances in Modeling Earth Systems*, **12 (3)**, e2019MS001 734.

- 612 Wofsy, J., and Z. Kuang, 2012: Cloud-resolving model simulations and a simple model of an
613 idealized Walker cell. *Journal of climate*, **25 (23)**, 8090–8107.
- 614 Woollings, T., M. Drouard, C. H. O'Reilly, D. M. Sexton, and C. McSweeney, 2023: Trends in the
615 atmospheric jet streams are emerging in observations and could be linked to tropical warming.
616 *Communications Earth & Environment*, **4 (1)**, 125.
- 617 Yang, W., R. Seager, and M. A. Cane, 2013: Zonal momentum balance in the tropical atmospheric
618 circulation during the global monsoon mature months. *Journal of the atmospheric sciences*,
619 **70 (2)**, 583–599.
- 620 Zhang, M., and Y. Huang, 2014: Radiative forcing of quadrupling CO₂. *Journal of Climate*, **27 (7)**,
621 2496–2508.
- 622 Zhang, Y., and S. Fueglistaler, 2019: Mechanism for increasing tropical rainfall unevenness with
623 global warming. *Geophysical Research Letters*, **46 (24)**, 14 836–14 843.
- 624 Zhang, Y., I. Held, and S. Fueglistaler, 2021: Projections of tropical heat stress constrained by
625 atmospheric dynamics. *Nature Geoscience*, **14 (3)**, 133–137.



Click here to access/download

Supplemental Material

WTG_project_JAS_SI_0622.pdf

